Mutational Analysis of a Nucleosidase Involved in Quorum-Sensing Autoinducer-2 Biosynthesis†

Jeffrey E. Lee,‡,§ Winnie Luong,‡,§ David J. T. Huang,‡ Kenneth A. Cornell,# Michael K. Riscoe,||,⊥ and P. Lynne Howell*,‡,§

Structural Biology and Biochemistry, Research Institute, Hospital for Sick Children, 555 University Avenue, Toronto, Ontario M5G 1X8, Canada, Department of Biochemistry, Faculty of Medicine, University of Toronto, Medical Sciences Building, Toronto, Ontario M5S 1A8, Canada, Department of Chemistry, Boise State University, 1910 University Drive, Boise, Idaho 83725-1520, Department of Chemistry, Portland State University, Portland, Oregon 97207, and Medical Research Service, RD-33, Veterans Affairs Medical Center, 3710 SW U.S. Veterans Hospital Road, Portland, Oregon 97021

Received March 17, 2005; Revised Manuscript Received May 25, 2005

ABSTRACT: 5′-Methylthioadenosine/*S*-adenosylhomocysteine nucleosidase (MTAN) is important in a number of cellular functions such as polyamine biosynthesis, methionine salvaging, biological methylation, and quorum sensing. The nucleosidase is found in many microbes but not in mammalian systems, thus making MTAN a broad-spectrum antimicrobial drug target. Substrate binding and catalytic residues were identified from the crystal structure of MTAN complexed with 5′-methylthiotubercidin [Lee, J. E., Cornell, K. A., Riscoe, M. K. and Howell, P. L. (2003) *J. Biol. Chem. 278* (10) 8761−8770]. The roles of active site residues Met9, Glu12, Ile50, Ser76, Val102, Phe105, Tyr107, Phe151, Met173, Glu174, Arg193, Ser196, Asp197, and Phe207 have been investigated by site-directed mutagenesis and steady-state kinetics. Mutagenesis of residues Glu12, Glu174, and Asp197 completely abolished activity. The location of Asp197 and Glu12 in the active site is consistent with their having a direct role in enzyme catalysis. Glu174 is suggested to be involved in catalysis by stabilizing the transition state positive charge at the O3′, C2′, and C3′ atoms and by polarizing the 3′-hydroxyl to aid in the flow of electrons to the electron withdrawing purine base. This represents the first indication of the importance of the 3′-hydroxyl in the stabilization of the transition state. Furthermore, mutation of Arg193 to alanine shows that the nucleophilic water is able to direct its attack without assistance from the enzyme. This mutagenesis study has allowed a reevaluation of the catalytic mechanism.

Bacteria are known to release and monitor the levels of a variety of chemical signals called autoinducers. These signals allow bacteria to estimate population density and to coordinate gene expression. Unlike other autoinducers that are unique to a particular bacterial species, autoinducer-2 (AI-2)[1] is common to most bacterial species. AI-2 was originally identified in *Vibrio harveyi* as one of two autoinducer systems that control bioluminescence in response to cell population density (*1*, *2*) and has been proposed to be a universal chemical messenger for interbacterial species communications (*3*−*5*). AI-2 is synthesized from *S*-adenosylmethionine (Figure 1). Donation of the methyl group from *S*-adenosylmethionine generates *S*-adenosylhomocysteine (AdoHcy), which is subsequently hydrolyzed by 5′-methylthioadenosine/*S*-adenosylhomocysteine nucleosidase (MTAN) (E. C. 3.2.2.9) to yield adenine and *S*-ribosylhomocysteine (SRH) (*6*). SRH is then converted to 4,5-dihydroxy-2,3-pentanedione (DPD) and homocysteine using the enzyme LuxS (*5*). The AI-2 response in different bacterial species can be triggered by at least two different derivatives of DPD (Figure 1). In *V. harveyi*, DPD cyclizes with the addition of borate to form (2*S*,4*S*)-2-methyl-2,3,3,4-tetrahydroxytetrahydrofuran-borate (*7*, *8*), while in *Salmonella typhimurium*, DPD cyclizes without the addition of borate to (2*R*,4*S*)-2-methyl-2,3,3,4-tetrahydroxytetrahydrofuran (*9*). In fact, borate inhibits the AI-2 response in *S. typhimurium* (*9*). Since DPD and AI-2 production are regulated at the level of SRH availability and not at the level of LuxS expression (*10*), MTAN is a critical enzyme in the biosynthesis of both quorum sensing AI-2 molecules. In addition, MTAN and AdoHcy are involved in the regulation of biological methylation though a negative feedback inhibition mechanism of AdoMet-dependent methyl transferases (*11*).

† This work is supported by a grant from the Canadian Institute for Health Research (CIHR, #43998) to P.L.H. K.A.C. and M.K.R. received financial support from the U.S. Veterans Affairs Medical Research Program and the United States Department of Agriculture (#02−0047). P.L.H. and J.E.L. are recipients of CIHR Investigator and Doctoral Research Awards, respectively. D.J.T.H. and W.L. were supported by summer studentships from the Natural Sciences and Engineering Research Council of Canada (NSERC).

* To whom correspondence should be addressed. Tel: (416) 813-5378. Fax: (416) 813-5379. E-mail: howell@sickkids.ca.

‡ Hospital for Sick Children.

§ University of Toronto.

Boise State University.

|| Portland State University.

⊥ Veterans Affairs Medical Center.

[1] Abbreviations: autoinducer-2, (AI-2); MTA, 5′-methylthioadenosine; AdoHcy, *S*-adenosylhomocysteine; MTAN, MTA/AdoHcy nucleosidase; MTR, 5-methylthioribose; SRH, *S*-ribosylhomocysteine; MTAP, MTA phosphorylase; PNP, purine nucleoside phosphorylase; NH, nucleoside hydrolase; CD, circular dichroism; WT, wild-type; NP-1, nucleoside phosphorylase-1; INT, 2-(4-iodophenyl)-3-(4-nitrophenyl)-5-phenyltetrazolium chloride; AI-2, autoinducer-2; DPD, 4,5-dihydroxy-2,3-pentanedione.

10.1021/bi050493q CCC: $30.25
Published on Web 07/29/2005

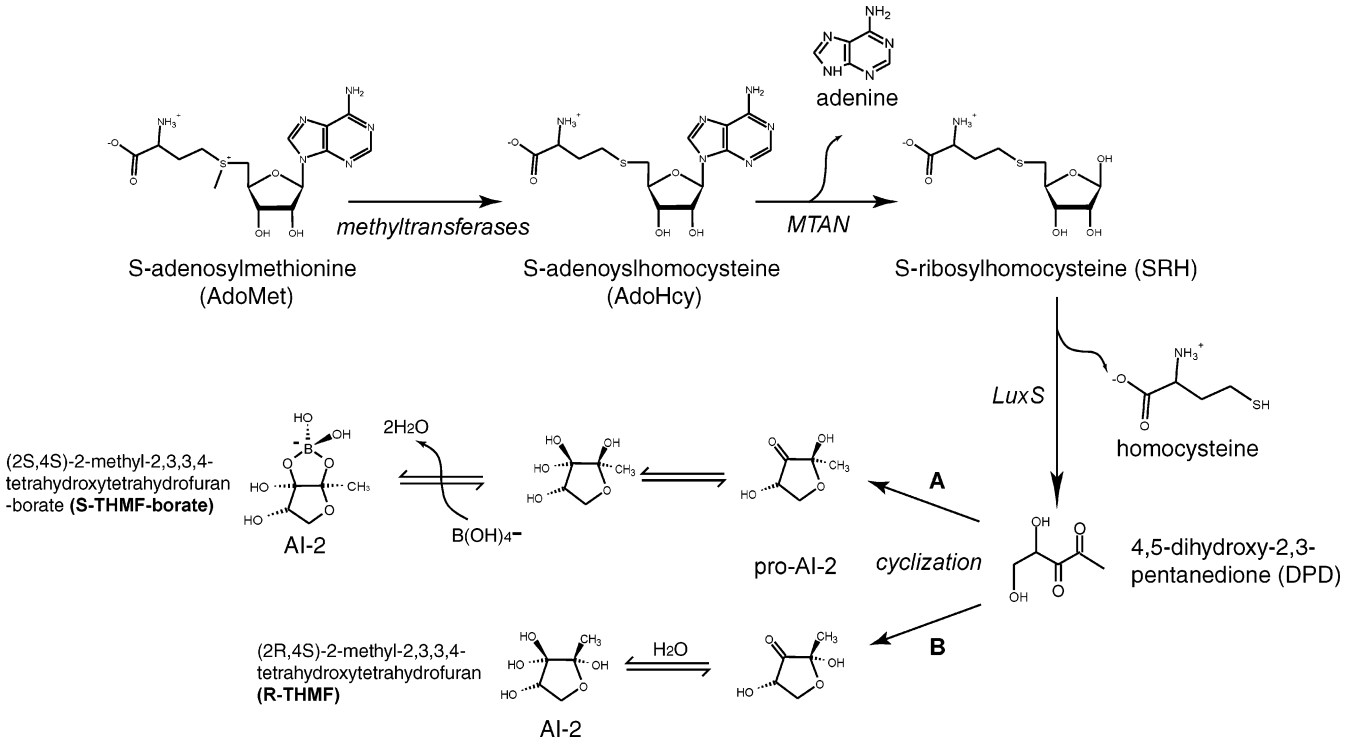

FIGURE 1: Biosynthetic pathways of autoinducer-2 (AI-2). Methyl transferases catalyze the transfer of a methyl group from *S*-adenosylmethionine (AdoMet) to a donor molecule to form *S*-adenosylhomocysteine (AdoHcy). MTA/AdoHcy nucleosidase (MTAN) quickly converts AdoHcy to adenine and *S*-ribosylhomocysteine (SRH). SRH is then catabolized by LuxS to form homocysteine and 4,5-dihydroxy-2,3-pentanedione (DPD). DPD spontaneously cyclizes and rearranges in two possible pathways to form the AI-2 signaling molecules. In *V. harveyi* (branch A), the addition of borate ($B(OH)_4^-$) to pro-AI-2 forms a cyclic borate diester as the AI-2 signaling molecule (*8*). However in *S. typhimurium* (branch B), DPD cyclizes and rearranges to form a chemically distinct borate-free AI-2 in the presence of water (*9*).

MTA/AdoHcy nucleosidase also irreversibly cleaves MTA to form 5-methylthioribose and adenine. This enzymatic function of MTAN is involved in the salvage of methionine and polyamine biosynthesis. Theoretically, inhibition of MTAN would lead to a build up of MTA. As a consequence, methionine salvage is abolished directly, and by negative feedback the polyamine biosynthetic enzymes are inhibited (*12*−*15*). Interestingly, both MTA and AdoHcy are catabolized differently in mammalian and microbial systems. In mammals and some microbes, MTA is broken down by MTA phosphorylase to adenine and 5-methylthioribose-1-phosphate, while AdoHcy is degraded by AdoHcy hydrolase to homocysteine and adenosine. Many microbes are devoid of MTA phosphorylase and AdoHcy hydrolase, and in these cases MTAN is the sole enzyme to breakdown both MTA and AdoHcy. Gene disruption studies on the pathogenic bacteria *Haemophilus influenzae*, *Streptococcus pneumoniae*, *Streptococcus pyogenes*, and *Enterococcus faecalis* have shown that mutations to the *pfs* gene are likely lethal (*16*). Given the importance of MTAN in cell survival and its specificity toward microbes, MTA/AdoHcy nucleosidase has been targeted for the design of antimicrobial therapeutic agents (*14*, *15*).

The structure of MTA/AdoHcy nucleosidase has been solved in the presence of adenine and the inhibitors: 5′-methylthiotubercidin (MTT), formycin A (FMA), 5′-methylthio-immucillin A (MT-ImmA), and 5′-methylthio-4′-deoxy-1′-aza-2′-deoxy-1′-(9-methylene)-immucillin A (MT-DADMe-ImmA) (*17*−*19*). These structures showed that the active site can be divided into three separate regions, the purine, ribose, and 5′-alkylthio binding subsites. The reactions catalyzed by MTAN are similar to those catalyzed by other nucleoside hydrolases (NH) and also nucleoside phosphorylases. Enzymes in both of these classes cleave the C−N bond between the purine or pyrimidine base and the ribose. Although both enzyme families catalyze similar reactions, MTAN is structurally similar to the nucleoside phosphorylase-1 (NP-1) family of enzymes and not to the nucleoside hydrolases (*18*). On the basis of the similarity of the structure and reactions catalyzed, MTAN has been proposed to have a similar catalytic schema as the NP-1 enzymes (*18*, *19*). These enzymes are proposed to undergo a dissociative two-step S_N1-type reaction (*20*−*23*). Although the catalytic mechanism of the NP-1 family of enzymes has been well studied, there are several features of the MTAN mechanism that appear to differ from the nucleoside phosphorylases and hydrolases that need to be examined. There is no direct experimental evidence to implicate residues involved in stabilization of the oxacarbenium-like ion or the role of residues involved in substrate specificity and catalysis. To further explore the catalytic mechanism of MTAN, we made single amino acid substitutions in the active site to examine the role of each residue. This is the first direct mutational and kinetic study of active site residues in MTAN. The results have allowed us to reexamine the enzyme mechanism of MTA/AdoHcy nucleosidase.

EXPERIMENTAL PROCEDURES

Site-Directed Mutagenesis and Protein Preparation. The QuikChange site-directed mutagenesis kit (Strategene) was used to generate the following mutants: Met9Ala, Glu12Ala, Glu12Gln, Ile50Ala, Ser76Ala, Val102Ala, Phe105Ala,

Tyr107Ala, Phe151Ala, Met173Ala, Glu174Ala, Glu174Gln, Arg193Ala, Ser196Ala, Asp197Ala, Asp197Asn, and Phe207Ala. Mutagenic primers were designed according to the QuikChange protocol and synthesized in a 40-nmol scale with cartridge purification at The Centre for Applied Genomics, Hospital for Sick Children. Plasmid DNA was isolated using the QIAprep spin miniprep kits (Qiagen). All mutants were confirmed by double-stranded DNA sequencing (ACGT Corp). The plasmid containing the desired mutation was transformed into *Escherichia coli* BL21 (DE3) cells by heat shock at 42 °C. All mutants were overexpressed and purified as reported previously (*24*). Electrospray ionization mass spectrometry on a Micromass ESI-qTOF mass spectrometer was performed on all purified mutants for quality control at the Advanced Protein Technology Centre, Hospital for Sick Children.

Circular Dichroism Spectroscopy. Purified MTAN enzymes were characterized by circular dichroism (CD) spectroscopy on an AVIV model 62DS spectrometer to determine whether any gross changes in stability and secondary structure occurred as a consequence of the mutations. A 5 μM solution of enzyme in 25 mM potassium phosphate pH 7.0 was scanned from 200 to 270 nm in a 0.1-cm path length cuvette. Five spectra were acquired and averaged at 25 °C using 1-nm steps and an integration time of 1 s. To compare their relative stabilities, the thermal denaturation of the mutants was monitored as a function of ellipticity at 222 nm. The temperature was increased from 25 to 95 °C in 2 °C increments with 1 min equilibration. Each temperature point was acquired using an integration time of 15 s.

Enzyme-Coupled Spectrophotometric Assay. The activity of the wild type (WT) and each mutant enzyme was compared and quantified by measuring the amount of adenine released using a xanthine oxidase-coupled spectrophotometric assay as previously described (*25*). All reagents for the kinetic assay were purchased from Sigma-Aldrich Chemicals (St. Louis, MO). The concentration of either 5′-methylthioadenosine or *S*-adenosylhomocysteine was varied between 0.75 and 24.1 μM. Reactions were carried out in 50 mM potassium phosphate pH 7.0, 0.28 units of grade III buttermilk xanthine oxidase, 1 mM 2-(4-iodophenyl)-3-(4-nitrophenyl)-5-phenyltetrazolium chloride (INT), and 0.025−70 μg of MTAN. The reaction was monitored at 470 nm on a Biochrome Ultrospec 2100 UV/Vis spectrophotometer outfitted with the SWIFT II enzyme kinetics software. Changes in absorbance were converted to the amount of adenine released using the molar absorption coefficient (15 400 M^{-1} cm^{-1} at pH 7.0). All enzyme reactions had a final reaction volume of 800 μL and were performed in triplicate at room temperature. The kinetic data were fit to the Michaelis-Menton equation using the SigmaPlot Enzyme Kinetics module.

RESULTS

Selection of Mutagenic Targets. The structures of *E. coli* MTAN complexed with 5′-methylthiotubercidin and formycin A allowed the identification of potential binding and catalytic residues in the purine, ribose, and 5′-alkylthio binding sites (*19*). Residues targeted for mutagenesis formed either a hydrogen bond or made van der Waals contacts

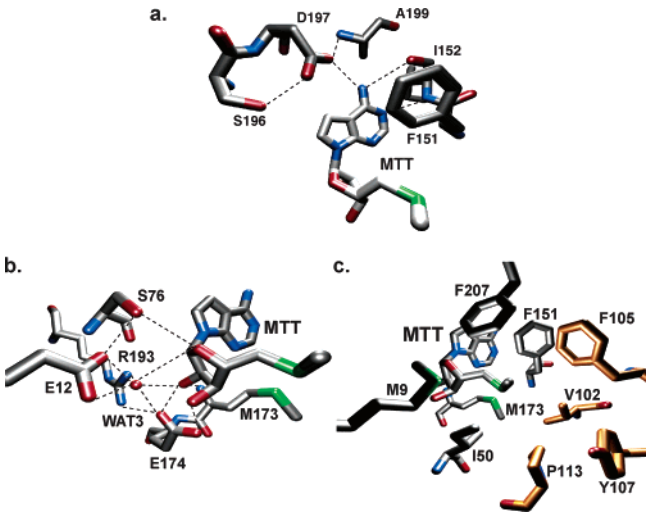

FIGURE 2: *E. coli* MTA/AdoHcy nucleosidase active site. Stick diagram of the (a) purine, (b) ribose, and (c) 5′-alkylthio binding subsites. Hydrogen bonds are denoted by black dashed lines, and residues donated from a neighboring subunit are colored in orange. The active site model is based on the atomic coordinates for the MTAN−MTT complex (PDB code: 1NC1). Figure was prepared using VMD (*38*).

directly with the substrate (Figures 2 and 3). Accordingly, residues Phe151, Ser196, and Asp197 in the purine binding site; Glu12, Ser76, Met173, Glu174, and Arg193 in the ribose binding site; and Met9, Ile50, Val102, Phe105, Tyr107, and Phe207 in the 5′-alkylthio binding site were targeted for mutagenesis. In designing the mutants, amino acid substitutions were kept as isosteric as possible to minimize any structural variation that may occur in the active site as a consequence of the mutation.

Assessing Structural Integrity of MTAN Mutants. Overexpression of the WT and mutant MTAN in the *E. coli* BL21 (DE3) strain led to the production of ∼30 mg of enzyme per liter of cells. The structural integrity of the MTAN mutants was evaluated in three ways. First, the oligomeric state of the mutants was evaluated using analytical gel filtration chromatography. Analysis of the retention volumes on a FPLC Superdex-200 10/30 HR column indicated that all mutants exist as the expected dimer (data not shown). Second, the CD spectra of WT and mutant *E. coli* MTAN were measured from 200 to 270 nm. All spectra displayed the same curve shape with minima at 208 and 222 nm as is characteristic of enzymes containing significant α-helical secondary structure (data not shown). All spectra were generally superimposable with the exceptions of Glu12Gln, Ser196Ala, Met173Ala, and Phe207Ala, suggesting that the relative content of α-helical and β-sheet had not changed significantly as a result of the targeted point mutation. The Glu12Gln, Met173Ala, Ser196Ala, and Phe207Ala mutants appear to have gained α-helicity in comparison to the WT protein. It should be noted, however, that CD spectra have a strong dependence on the concentration of the protein. Although every attempt was made to accurately measure the protein concentration, given the low concentrations used there may be measurement errors that account for the deviations of the mutants from WT in the CD spectra. Third, the CD signal at 222 nm was monitored as the proteins were thermally denatured from 25 to 95 °C. The WT spectra displayed a sigmoidal curve with an apparent T_m of 68 °C.

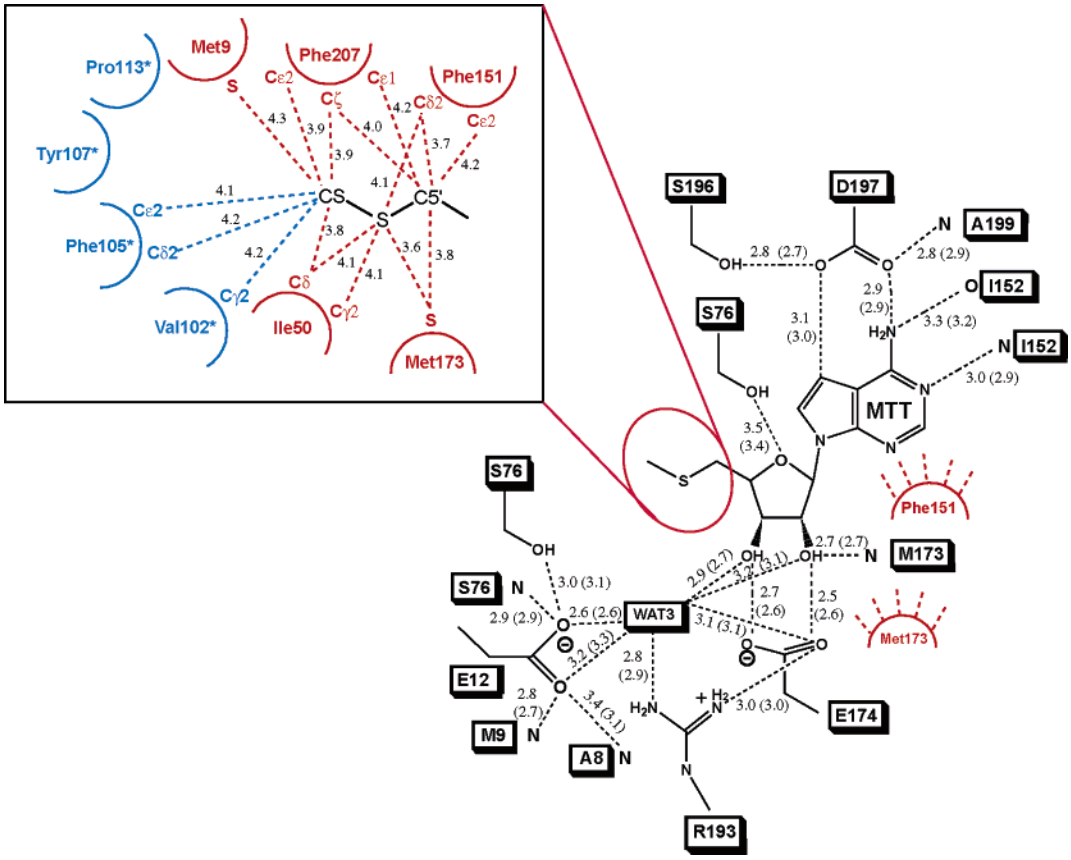

FIGURE 3: Active site schematic of *E. coli* MTA/AdoHcy nucleosidase. Protein−protein and protein−ligand hydrogen bonds are shown by dashed lines. Residues that are donated from the neighboring subunit are colored blue and labeled with an asterisk. van der Waals interactions between the inhibitor (MTT) and the enzyme are indicated by both red and blue labeled residues. All distances shown are in angstroms (Å), with numbers in and outside the brackets referring to hydrogen bond distances in monomer A and B of the MTAN−MTT structure, respectively.

Table 1: Kinetic Parameters for Purine Binding Subsite Mutants

enzyme	substrate	K_m (μM)	k_{cat} (s^{-1})	k_{cat}/K_m ($s^{-1}\,\mu M^{-1}$)	catalytic efficiency (%)	apparent T_m[a] (°C)
WT	MTA	0.8 ± 0.2	3.0 ± 0.1	3.6 ± 0.7	100	68
	AdoHcy	1.3 ± 0.2	2.6 ± 0.1	2.1 ± 0.3	100	
Phe151Ala	MTA	22 ± 2	(3.7 ± 0.1) × 10^{-1}	(1.7 ± 0.2) × 10^{-2}	0.5	68
	AdoHcy	37 ± 4	(1.4 ± 0.1) × 10^{-1}	(3.8 ± 0.4) × 10^{-3}	0.2	
Ser196Ala	MTA	2.9 ± 0.6	(2.3 ± 0.2) × 10^{-1}	(8.1 ± 1.9) × 10^{-2}	2.3	66
	AdoHcy	1.7 ± 0.3	(1.4 ± 0.1) × 10^{-1}	(8.4 ± 1.5) × 10^{-2}	4.0	
Asp197Ala	MTA		inactive[b]			70
	AdoHcy		inactive			
Asp197Asn	MTA		inactive[b]			72
	AdoHcy		inactive			

[a] Temperature at which half the signal is lost at 222 nm. [b] Activity was too low to fit the curve.

The majority of mutants studied here exhibited thermal stabilities comparable to WT (Tables 1−3). The Met9Ala, Ile50Ala, Met173Ala, Arg193Ala, Asp197Asn, and Phe207Ala mutants appeared to have increased stability with apparent T_m's ranging between 71 and 75 °C, and mutations to Glu12 and Glu174 resulted in decreased stability with apparent T_m's between 63 and 65 °C. All transitions were found to be cooperative and irreversible. Although thermodynamic data cannot be obtained from irreversible thermal melts, the apparent T_m's serve as a simple way of comparing the stabilities of WT and mutant enzymes. All enzymes were heat tolerant to ~60 °C, and therefore any variations in the thermal stabilities are unlikely to affect the enzyme activity measured at room temperature (22 °C).

Kinetic Characterization of MTAN Mutants. WT and mutant MTAN activities were quantified spectrophotometrically by monitoring the production of formazan at 470 nm (*25*). De Groot and Noll had previously shown that the dehydrogenase counterfunction of xanthine oxidase acting on a molecule of deaminated adenine (hypoxanthine) led to the reduction of two molecules of INT to give a colored formazan product (*26*). All mutant kinetics were measured at the pH optima (pH = 7.0) (*27*). All active enzymes also displayed linear kinetics, and the initial velocity data were fit to the Michaelis−Menten equation to determine the kinetic parameters, K_m and V_{max}. k_{cat} was calculated using V_{max}.

WT and each MTAN mutant were assayed using both natural substrates, MTA and AdoHcy, over a substrate

Table 2: Kinetic Parameters for Ribose Binding Subsite Mutants

enzyme	substrate	K_m(μM)	k_{cat} (s^{-1})	k_{cat}/K_m ($s^{-1}\,\mu M^{-1}$)	catalytic efficiency (%)	apparent T_m[a] (°C)
WT	MTA	0.8 ± 0.2	3.0 ± 0.1	3.6 ± 0.7	100	68
	AdoHcy	1.3 ± 0.2	2.6 ± 0.1	2.1 ± 0.3	100	
Glu12Ala	MTA			inactive[b]		64
	AdoHcy			inactive		
Glu12Gln	MTA			inactive[b]		63
	AdoHcy			inactive		
Ser76Ala	MTA	2.7 ± 0.4	1.3 ± 0.1	0.5 ± 0.1	13.4	70
	AdoHcy	1.9 ± 0.3	$(9.3 \pm 0.3) \times 10^{-1}$	0.5 ± 0.1	22.9	
Met173Ala	MTA	34 ± 3	$(7.2 \pm 0.3) \times 10^{-1}$	$(2.1 \pm 1.0) \times 10^{-2}$	0.6	71
	AdoHcy	$(4.9 \pm 1.8) \times 10^{2}$	0.8 ± 0.2	$(1.7 \pm 0.8) \times 10^{-3}$	0.1	
Glu174Ala	MTA			inactive[b]		65
	AdoHcy			inactive		
Glu174Gln	MTA			inactive[b]		65
	AdoHcy			inactive		
Arg193Ala	MTA	3.2 ± 0.4	1.5 ± 0.1	0.5 ± 0.1	12.9	72
	AdoHcy	2.0 ± 0.3	1.2 ± 0.1	0.6 ± 0.1	28.1	

[a] Temperature at which half the signal is lost at 222 nm. [b] Activity was too low to fit the curve.

Table 3: Kinetic Parameters for 5′-Alkylthio Binding Subsite Mutants

enzyme	substrate	K_m (μM)	k_{cat} (s^{-1})	k_{cat}/K_m ($s^{-1}\,\mu M^{-1}$)	catalytic efficiency (%)	apparent T_m[a] (°C)
WT	MTA	0.8 ± 0.2	3.0 ± 0.1	3.6 ± 0.7	100	68
	AdoHcy	1.3 ± 0.2	2.6 ± 0.1	2.1 ± 0.3	100	
Met9Ala	MTA	1.4 ± 0.2	$(6.3 \pm 0.3) \times 10^{-1}$	0.5 ± 0.1	12.6	71
	AdoHcy	1.0 ± 0.1	$(3.7 \pm 0.2) \times 10^{-1}$	0.4 ± 0.1	18.6	
Ile50Ala	MTA	7.1 ± 0.4	3.0 ± 0.1	$(4.2 \pm 0.3) \times 10^{-1}$	11.8	75
	AdoHcy	3.7 ± 0.5	1.8 ± 0.1	0.5 ± 0.1	23.3	
Val102Ala	MTA	3.0 ± 0.2	10.2 ± 0.2	3.4 ± 0.3	95.0	67
	AdoHcy	1.9 ± 0.2	9.1 ± 0.2	4.9 ± 0.4	233	
Phe105Ala	MTA	3.3 ± 0.2	10.2 ± 0.2	3.1 ± 0.2	87.4	66
	AdoHcy	2.8 ± 0.3	7.5 ± 0.2	2.7 ± 0.3	128	
Tyr107Phe	MTA	2.2 ± 0.2	2.5 ± 0.1	1.2 ± 0.1	32.2	67
	AdoHcy	1.7 ± 0.3	2.0 ± 0.1	1.2 ± 0.2	58.1	
Phe207Ala	MTA	1.7 ± 0.2	$(1.3 \pm 0.1) \times 10^{-1}$	$(8.0 \pm 1.0) \times 10^{-2}$	2.2	72
	AdoHcy	5.5 ± 0.6	$(3.1 \pm 0.1) \times 10^{-1}$	$(5.6 \pm 0.6) \times 10^{-2}$	2.7	

[a] Temperature at which half the signal is lost at 222 nm.

concentration range of 0.75−24.1 μM (Tables 1−3). WT MTAN has k_{cat}/K_m values of (3.6 ± 0.7) $s^{-1}\,\mu M^{-1}$ and (2.1 ± 0.3) $s^{-1}\,\mu M^{-1}$ for MTA and AdoHcy, respectively. The K_m values of MTA and AdoHcy were consistent with reported values determined from a radioactive kinetic assay (*27*, *28*). Of the three residues mutated in the purine binding site, the largest kinetic effect is observed for mutations to Asp197 (Table 1). The Asp197Ala and Asp197Asn mutants were completely inactive. Mutations to Phe151 and Ser196 retained <1 and ∼2% catalytic efficiency compared to WT, respectively. Of the five residues mutated in the ribose binding site, substitutions to Glu12 and Glu174 completely abolished activity. Met173Ala exhibited <1% catalytic efficiency compared to WT, with a larger change in K_m than k_{cat}. Ser76Ala and Arg193Ala mutations resulted in catalytic efficiencies of ∼13−28% for MTA and AdoHcy. Mutations to 5′-alkylthio binding site residues provided mixed kinetic results. The Met9Ala substitution resulted in a small increase in K_m but larger decreases in k_{cat}. The Ile50Ala and Phe207Ala substitutions resulted in K_m increases ranging from 2.1−8.9-fold for MTA and AdoHcy, while k_{cat} remained virtually unchanged. Interestingly, Tyr107Phe had similar k_{cat} values toward MTA and AdoHcy as the WT MTAN, although the K_m for MTA and AdoHcy increased only ∼2.8- and 1.3-fold, respectively. Val102Ala and Phe105Ala mutants exhibited an overall increase of 233 and 128% in k_{cat}/K_m for AdoHcy, respectively. The catalytic efficiencies of Val102Ala and Phe105Ala for MTA were similar to WT.

DISCUSSION

Role of Active Site Residues in Substrate Binding. The Michaelis constant, K_m, is often used as a measure of substrate affinity because the rate of the dissociation of the enzyme−substrate complex (ES) to free enzyme and substrate (k_{-1}) is assumed to be much faster than the rate of catalysis (k_{cat}). Previous characterizations of WT MTAN using a radioactive assay revealed a bell-shaped pH dependence of k_{cat} but a pH independence of K_m (*27*). This suggests that k_{-1} is significantly larger than k_{cat}, and assuming that this holds true for all our mutants, measurements of K_m would provide a good measure of substrate affinity.

Purine Binding Subsite Residues. Residues Phe151 and Asp197 are likely the key determinants for purine binding. The mutation of Phe151 to alanine resulted in significantly reduced catalytic efficiencies for MTA and AdoHcy, due to changes in both K_m and k_{cat}, but predominantly K_m. This reflects the loss of $\pi-\pi$ electron interactions between the aromatic rings of Phe151 and adenine (Figure 2a). While the primary role of Asp197 is thought to be in catalysis as the general acid, this residue also likely has a role in substrate binding and substrate recognition. The hydrogen bond made between Asp197 and the adenine N7 and N6 atoms is thought to provide substrate specificity toward nucleosides with 6-aminopurine bases, as MTAN is able to discriminate between the 6-oxopurine, 5′-methylthioinosine, and MTA (*28*).

Ribose Binding Subsite Residues. The mutagenesis data confirm the importance of Met173 and potentially Glu174 in binding. Met173 helps to anchor the ribose moiety by packing its side chain against the hydrophobic face of the ribose and 5′-alkylthio tail, and by participation in a hydrogen bond between its main chain amide nitrogen and the ribosyl 2′-hydroxyl (Figures 2b and 3). Interestingly, the K_m-(Met173Ala)/K_m(WT) ratio for AdoHcy was ~10 times higher than the K_m(Met173Ala)/K_m(WT) ratio for MTA. This suggests the side chain of Met173 and the anchoring of the ribose are critical for the binding of AdoHcy. Met173 is conserved in many MTAN species, and an equivalent methionine residue in other NP-1 enzymes makes similar interactions. Alanine substitution of the equivalent methionine in PNP results in a 200-fold decrease in K_m (*29*), a result that coupled with our current data suggests that the methionine's role in ribose binding is likely conserved throughout the NP-1 family of enzymes. Glu174 interacts with the ribose via two hydrogen bonds from its Oϵ1 and Oϵ2 atoms to the 2′- and 3′-hydroxyls, respectively (Figures 2b and 3). Alanine and glutamine mutations of the strictly conserved Glu174 residue completely abolished enzyme activity, suggesting that Glu174 may have roles in both catalysis and binding (see below).

5′-Alkylthio Binding Subsite Residues. Our mutational analyses within the 5′-alkylthio binding subsite show that mutations to Ile50Ala, Val102Ala, Phe105Ala, and Tyr107Phe have modest effects on both K_m and k_{cat}. These residues play only minor roles in the binding of MTA or AdoHcy. The modest changes in K_m of Tyr107Phe compared to WT (2−3-fold increase) rules out a role for the Tyr107 Oη in binding the α-carboxyl or α-amino group of AdoHcy. Previous crystal structures of MTAN had suggested that AdoHcy binding may be accommodated due to the size of the 5′-alkylthio binding subsite and the presence of a hydrogen bond from either the α-carboxyl or the α-amino of AdoHcy to Tyr107 Oη (*18*, *19*). Met9 and Phe207 have also been implicated in binding the 5′-alkylthio moiety as the sulfur of Met9 is 4.3 Å away from the CS atom, and the Cϵ1, Cϵ2, and Cζ atoms of Phe207 make van der Waals contacts to the substrate's C5′ and CS atoms (Figures 2b and 3). Mutations to Met9 and Phe207 result in decreases in catalytic efficiencies (82.4−97.8%). These decreases appear to be primarily due to k_{cat} and not K_m, suggesting that these residues play a role in catalysis. The residues in the 5′-alkylthio binding subsite do not play major roles in substrate binding. Collectively, these apolar or aromatic 5′-alkylthio binding site residues likely sequester the substrate from the solvent to improve the stability of the oxacarbenium-like ion. Oxacarbenium ions are extremely sensitive to water and are short-lived in aqueous solutions, with estimated lifetimes of $\sim 10^{-12}$ s (*30*). As seen in all MTAN−inhibitor complexes, the ribose and 5′-alkylthio binding sites are devoid of water, except for the nucleophilic water (Figure 2c). In general, the active sites of other NP-1 enzymes are also fairly dehydrated.

Role of Active Site Residues in Substrate Catalysis. The previously solved structures of MTAN reveal strong similarities in the overall structure and active site architecture to the nucleoside phosphorylase-1 family (*18*, *19*), which led us to propose that MTAN shares a similar catalytic rationale to the NP-1 family of enzymes (*18*). NP-1 enzymes are generally thought to proceed through a two-step dissociative S_N1-type mechanism (*23*, *29*, *31*). The first step involves proton donation to the N7 adenine ring from the enzyme to allow the formation of a hydrogen bond (Figure 4a). The electron withdrawing adenine base (electron pull) is stabilized by a flow of electrons from the ribose (electron push) (Figure 4b). This flow of electrons favors the elongation of the ribosidic bond and the build up of a positive charge on the ribose (Figure 4c). The transition state structure of MTAN, as predicted by kinetic isotope effects, shows partial positive charge buildup on the C1′, O3′, C3′, and C2′ atoms but not on the O4′ atom (*32*). Following the formation of the oxacarbenium-like ion, a nucleophilic attack occurs at the C1′ atom to form the products (Figure 4c,d). Plots of log V_{max} and log(V_{max}/K_m) as a function of pH for MTA reveal two essential ionizable groups for catalysis, with apparent pK_a of 5.6 and 8.2 (*27*). Our mutational analysis of MTAN has allowed a reevaluation of the leaving group activation, flow of electrons and oxacarbenium stabilization, and nucleophilic activation and attack steps of catalysis.

Leaving Group Activation. The importance of the N7 atom in leaving group activation seems to be a recurring theme in the mechanism of acid-catalyzed cleavage of purine nucleosides (*33*) and in enzymes that cleave ribosidic linkages such as nucleoside hydrolases and nucleoside phosphorylases (*23*, *29*, *34*, 35). In MTAN, Asp197 is proposed to have a raised pK_a to facilitate the donation of a proton to the adenine N7 (Figure 4a). A raised pK_a for Asp197 is consistent with the pH profile of MTAN. The first ionizable group at physiological pH (pK_a = 8.2) has been previously suggested to be responsible for the activation of the leaving group (*27*). The hydrogen bond formed between the N7 and the Asp197 Oδ2 also aids catalysis by stabilizing the transition state as there is an increase in positive charge density at the N7 atom during bond cleavage (*29*). It is therefore not surprising that mutations of Asp197 to either alanine or asparagine resulted in the complete loss of enzyme activity, thus confirming its critical role in catalysis. Asp197 is definitely a key residue as mutations to residues Phe151, Ser196, and Phe207 that interact with Asp197 or the adenine base also showed a decrease in activity. Ser196 is important in stabilizing the aspartate side chain into a catalytically competent orientation, as the Oγ of Ser196 makes a hydrogen bond to the Oδ2 atom of Asp197 (Figures 2a and 3). Phe151 makes stabilizing base stacking interaction with the adenine base and is involved in the proper alignment of the adenine to the N7. Residue Phe207 is important in a disordered loop-to-helix transition. This transition extends the α6 helix by one turn and helps propagate a structural displacement to the β10 sheet on which the Asp197 side chain resides. The Phe207Ala substitution may affect the loop-to-helix transition, thereby preventing an optimal alignment of the catalytic acid. Site-directed mutagenesis was not able to definitively pinpoint whether Asp197 donates the proton or mediates the transfer. Further experiments will be necessary to unambiguously determine the exact role of Asp197 in enzyme catalysis.

Role of Glu174 in Electron Flow and Oxacarbenium Ion Stabilization. After N7 proton donation, the purine base is electron deficient and draws electrons from the ribose. Originally, the flow of electrons was thought to uniquely occur from the O4′ atom to the purine base. The transition state structure of MTAN now suggests that the flow of

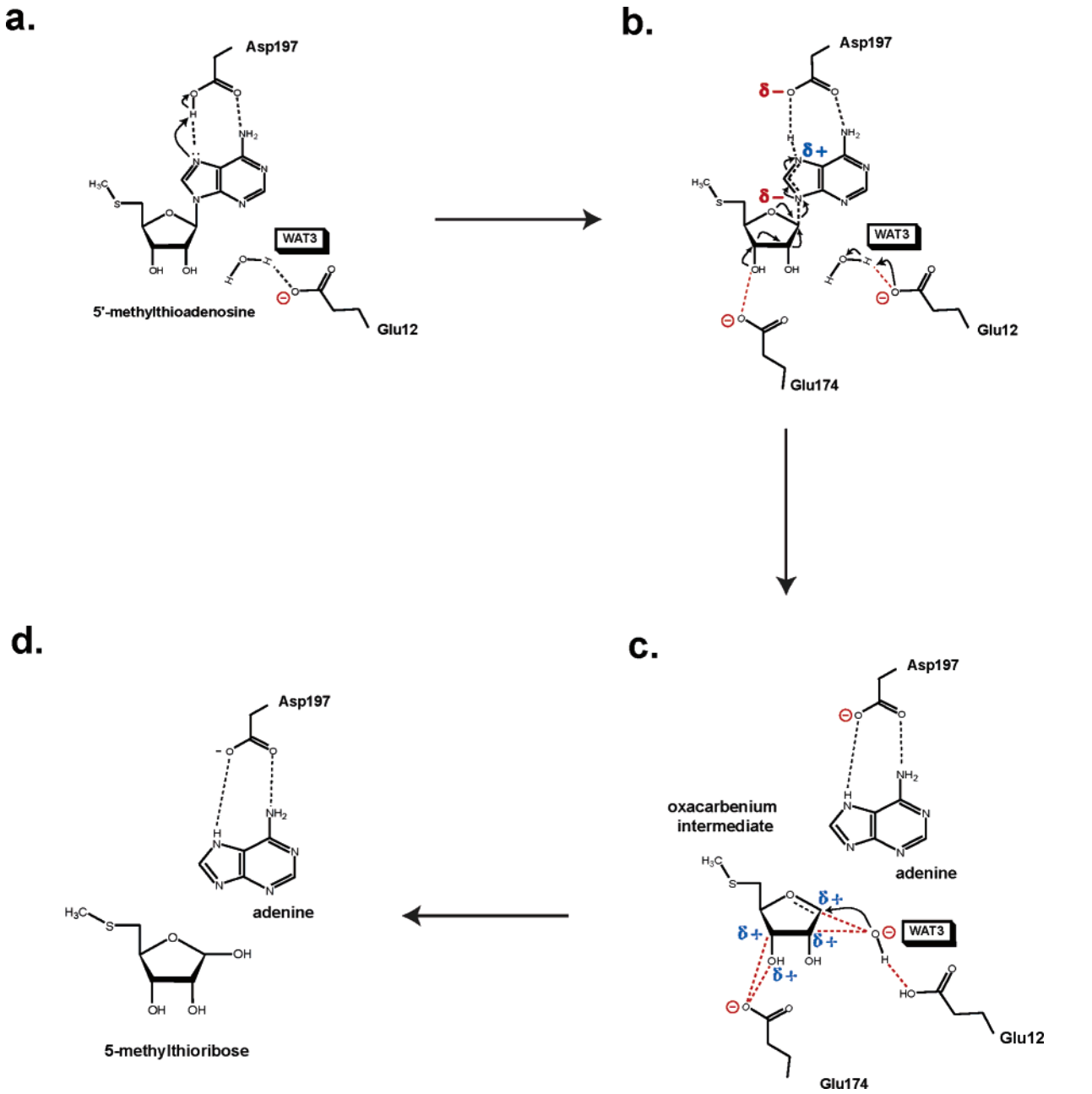

FIGURE 4: Proposed catalytic mechanism of MTA/AdoHcy nucleosidase. (a) Proton donation occurs from the catalytic acid (Asp197) to the N7 adenine. (b) The electron withdrawing purine base is stabilized by a flow of electrons from the ribose. This leads to ribosidic bond elongation, formation of the oxacarbenium-like ion, and partial positive charge buildup on the O3′, C3′, C2′, and C1′ atoms. (c) At the transition state, the leaving group is well removed and the oxacarbenium-like intermediate is stabilized by the nucleophilic water and Glu174. A Glu12 activated nucleophilic water attacks the anomeric carbon of the oxacarbenium intermediate to form the products shown in (d). Hydrogen bond interactions are shown by dashed lines.

electrons occurs not just from the O4′ atom but also from the C1′, C2′, C3′, and O3′ atoms (*32*). The electron flow reduces the partial negative charge on the ribosyl O4′ and increases the partial positive charge on the C1′, C2′, C3′, and O3′ atoms. Calculations have shown that the deprotonation of either the 2′- or 3′-hydroxyl will increase the delocalization or flow of electrons (*32*). The 3′-hydroxyl is likely involved in catalysis, as previous inhibitor-kinetic studies have shown that the 3′-deoxyMTA substrate analogue is non-hydrolyzable (*27*). The 2′-hydroxyl is likely not involved as the same experiments have shown that 2′-deoxyMTA retains 82% activity. In addition, the 3′-hydroxyl is ~2.7 Å away from the negatively charged carboxylate side chain of Glu174. Alanine and glutamine mutations to Glu174 have resulted in abolished catalytic activities. Taken together, the results suggest that Glu174 may ionize or deprotonate the 3′-hydroxyl to facilitate a push of electrons toward the electron-deficient purine base. This is the first time that the 3′-hydroxyl has been implicated in the catalysis of an NP-1 enzyme.

Previous crystal structures of MTAN complexed with potent transition state analogues suggest that the oxacarbenium-like ion may be stabilized at least in part by the nucleophilic water (*17*). The nucleophilic water (WAT3) is likely deprotonated by the catalytic base (Glu12) to a hydroxide, which acts as a stronger nucleophile. The activated water is in good position to stabilize the developing positive charge on the C1′ and C2′ atoms, as witnessed in

the MTAN-transition state analogue structures (*17*). The transition state structure of MTAN also suggests that a partial positive charge develops on the C3′ and O3′ positions (*32*). These atoms were originally thought to remain neutral during catalysis. The Oϵ2 of Glu174 is positioned 3.3 and 2.7 Å away from the C3′ and O3′ atoms, respectively, in the MTAN−MTT structure and is in excellent position to stabilize the partial positive charge buildup (Figures 2b and 3). The stabilization of the oxacarbenium ion by Glu174 is likely in addition to its role in the polarization or deprotonation of the 3′-hydroxyl. The polarization or deprotonation of the 3′-hydroxyl will likely reduce the negative charge density on Glu174. The partial negative charge rather than a formal negative charge on Glu174 may aid in stabilization as it potentially provides better electrostatic complementarity to the partial positive charge on the C3′ and O3′ atoms.

Nucleophilic Activation and Attack. Water is generally considered a poor nucleophile, so an enzyme-based activation of the nucleophile to a hydroxide is likely necessary. In the case of the nucleoside hydrolases, the nucleophilic water is activated with the help of a Ca^{2+} ion and an aspartate residue (*34*−*37*). In NP-1 enzymes, activation is not necessary as these enzymes use an anionic phosphate as the nucleophile. There are three residues in MTAN (Glu12, Glu174, and Arg193) that make hydrogen bonds to WAT3, the putative water nucleophile. Glu12 is the putative catalytic base, given its position to the nucleophilic water (∼2.7 Å average in all MTAN−inhibitor complexes) (Figures 2b and 3). Although it is possible that Glu174 could act as the catalytic base, the distance to WAT3 (3.1 Å) is much longer than the interactions observed between Glu12 and WAT3 (*27*). The inactivity of the Glu12 alanine and glutamine mutants reinforces the importance of this residue in catalysis. The identity of Glu12 as the catalytic base is consistent with the second essential ionizable group ($pK_a = 5.6$) found on the MTAN pH profile (*27*). Furthermore, mutation of Met9, whose amide nitrogen hydrogen bonds (2.8 Å) to the Glu12 Oϵ2 atom to stabilize the side chain, also led to a decrease in k_{cat} (Figure 3). Met9Ala may cause local perturbations to the main chain that prevent correct orientation of the catalytic base, Glu12. Furthermore, the kinetics show that activation of the nucleophile is critical for catalysis.

In the MTAN−MTT structure, the nucleophilic water is 3.6 Å from the anomeric carbon, and the conserved Arg193 was proposed to help direct the nucleophilic water toward the oxacarbenium-like ion (*19*). Comparison of the adenine and MTT-bound MTAN structures revealed a rotation about the Arg193 χ_4 bond to point the guanidinyl functional group toward the substrate (*19*). This conformational change allowed the guanidinyl group to form a hydrogen bond to the nucleophilic water and push WAT3 ∼0.4 Å closer to the anomeric carbon. A positively charged residue like Arg193 hydrogen bonding to the nucleophilic water would be expected to reduce the nucleophilicity of WAT3 and hinder catalysis. The kinetics of the Arg193Ala mutant showed only a modest 2-fold decrease in k_{cat} and K_m for both MTA and AdoHcy. Contrary to the original hypothesis, the kinetics show that WAT3 can likely direct its attack on the anomeric carbon without assistance from Arg193. As suggested by the structures of MTAN−MT−ImmA and MTAN−MT−DADMe−ImmA, the buildup of ribosyl positive charge may be the major force in attracting the nucleophilic water toward the substrate (*17*).

CONCLUSIONS

The site-directed mutagenesis studies presented here show that substrate binding is predominantly though adenine- and ribose-binding site residues. Mutations to Phe151 and Met173 resulted in the largest overall increase in K_m. Glu12, Glu174, and Asp197 were identified as active site residues essential for catalysis. The results are consistent with the previously proposed catalytic mechanism, with Glu12 and Asp197 serving functional roles as the catalytic base and acid, respectively. Glu174 was previously proposed to be solely involved in substrate binding, and as a consequence the lack of activity observed for the Glu174Ala and Glu174Gln mutants was rather surprising. Our site-directed mutagenesis-kinetic data coupled with previous inhibitor-kinetic studies, and the transition state structure of MTAN, suggest that in addition to a role in substrate binding Glu174 is involved in catalysis by polarizing the 3′-hydroxyl atom to aid in a flow of electrons to the purine base and also by stabilizing the transition state positive charge at the C3′ and O3′ atoms. This is the first time that the ribosyl O3′ atom has been proposed in the NP-1 family of enzymes to be important in catalysis. Our kinetic analysis also suggests that while Glu12 activates the nucleophilic water its attack on the anomeric carbon does not require the assistance of any additional active site residues.

ACKNOWLEDGMENT

The authors would like to acknowledge the insightful comments of the reviewers. The authors also wish to thank Dr. Avi Chakrabarty at the Ontario Cancer Institute for access to their circular dichroism spectropolarimeter and Dr. Yi-Min Shi and Li Zhang at the Advanced Protein Technology Centre at the Hospital for Sick Children for their efforts in mass spectrometry.

REFERENCES

1. Bassler, B. L., Wright, M., and Silverman, M. R. (1994) Multiple signalling systems controlling expression of luminescence in *Vibrio harveyi*: sequence and function of genes encoding a second sensory pathway, *Mol. Microbiol. 13*, 273−286.
2. Bassler, B. L., Wright, M., Showalter, R. E., and Silverman, M. R. (1993) Intercellular signalling in *Vibrio harveyi*: sequence and function of genes regulating expression of luminescence, *Mol. Microbiol. 9*, 773−786.
3. Miller, M. B., and Bassler, B. L. (2001) Quorum sensing in bacteria, *Annu. Rev. Microbiol. 55*, 165−199.
4. Schauder, S., and Bassler, B. L. (2001) The languages of bacteria, *Genes Dev. 15*, 1468−1480.
5. Surette, M. G., Miller, M. B., and Bassler, B. L. (1999) Quorum sensing in *Escherichia coli*, *Salmonella typhimurium*, and *Vibrio harveyi*: a new family of genes responsible for autoinducer production, *Proc. Natl. Acad. Sci. U.S.A. 96*, 1639−1644.
6. Duerre, J. A. (1962) A hydrolytic nucleosidase acting on S-adenosylhomocysteine and on 5′-methylthioadenosine, *J. Biol. Chem. 237*, 3737−3741.
7. Schauder, S., Shokat, K., Surette, M. G., and Bassler, B. L. (2001) The LuxS family of bacterial autoinducers: biosynthesis of a novel quorum-sensing signal molecule, *Mol. Microbiol. 41*, 463−476.
8. Chen, X., Schauder, S., Potier, N., Van Dorsselaer, A., Pelczer, I., Bassler, B. L., and Hughson, F. M. (2002) Structural identification of a bacterial quorum-sensing signal containing boron, *Nature 415*, 545−549.
9. Miller, S. T., Xavier, K. B., Campagna, S. R., Taga, M. E., Semmelhack, M. F., Bassler, B. L., and Hughson, F. M. (2004)

Salmonella typhimurium Recognizes a Chemically Distinct Form of the Bacterial Quorum-Sensing Signal AI-2, *Mol Cell 15*, 677−687.
10. Beeston, A. L., and Surette, M. G. (2002) pfs-dependent regulation of autoinducer 2 production in Salmonella enterica serovar Typhimurium, *J. Bacteriol. 184*, 3450−3456.
11. Borchardt, R. T., Creveling, C. R., and Ueland, P. M. (1986) *Biological Methylation and Drug Design-Experimental and Clinical Roles of S-Adenosylmethionine*, Humana Press, Clifton, NJ.
12. Pajula, R. L., and Raina, A. (1979) Methylthioadenosine, a potent inhibitor of spermine synthase from bovine brain, *FEBS Lett. 99*, 343−345.
13. Raina, A., Tuomi, K., and Pajula, R. L. (1982) Inhibition of the synthesis of polyamines and macromolecules by 5′-methylthioadenosine and 5′-alkylthiotubercidins in BHK21 cells, *Biochem. J. 204*, 697−703.
14. Riscoe, M. K., Ferro, A. J., and Fitchen, J. H. (1989) Methionine recycling as a target for antiprotozoal drug development, *Parasitol. Today 5*, 330−333.
15. Sufrin, J. R., Meshnick, S. R., Spiess, A. J., Garofalo-Hannan, J., Pan, X. Q., and Bacchi, C. J. (1995) Methionine recycling pathways and antimalarial drug design, *Antimicrob. Agents Chemother. 39*, 2511−2515.
16. Brett, P. J., Vasu, S. K., Grant, C. C. R., Levin, J. C., and McKenzie, D. T. (2002) in *42nd Interscience Conference on Antimicrobial Agents and Chemotherapy*, p F740, San Diego.
17. Lee, J. E., Singh, V., Evans, G. B., Tyler, P. C., Furneaux, R. H., Cornell, K. A., Riscoe, M. K., Schramm, V. L., and Howell, P. L. (2005) Structural rationale for the affinity of pico- and femtomolar transition state analogues for *E. coli* 5′-methylthioadenosine/S-adenosylhomocysteine nucleosidase., *J. Biol. Chem. 280*, 18274−18282.
18. Lee, J. E., Cornell, K. A., Riscoe, M. K., and Howell, P. L. (2001) Structure of *E. coli* 5′-methylthioadenosine/S-adenosylhomocysteine nucleosidase reveals similarity to the purine nucleoside phosphorylases, *Structure 9*, 941−953.
19. Lee, J. E., Cornell, K. A., Riscoe, M. K., and Howell, P. L. (2003) Structure of *Escherichia coli* 5′-methylthioadenosine/ S-adenosylhomocysteine nucleosidase inhibitor complexes provide insight into the conformational changes required for substrate binding and catalysis, *J. Biol. Chem. 278*, 8761−8770.
20. Kline, P. C., and Schramm, V. L. (1993) Purine nucleoside phosphorylase. Catalytic mechanism and transition-state analysis of the arsenolysis reaction, *Biochemistry 32*, 13212−13219.
21. Lewandowicz, A., and Schramm, V. L. (2004) Transition state analysis for human and Plasmodium falciparum purine nucleoside phosphorylases, *Biochemistry 43*, 1458−1468.
22. Appleby, T. C., Erion, M. D., and Ealick, S. E. (1999) The structure of human 5′-deoxy-5′-methylthioadenosine phosphorylase at 1.7 Å resolution provides insights into substrate binding and catalysis, *Structure 7*, 629−641.
23. Erion, M. D., Stoeckler, J. D., Guida, W. C., Walter, R. L., and Ealick, S. E. (1997) Purine nucleoside phosphorylase. 2. Catalytic mechanism, *Biochemistry 36*, 11735−11748.
24. Lee, J. E., Cornell, K. A., Riscoe, M. K., and Howell, P. L. (2001) Expression, purification, crystallization and preliminary X-ray analysis of *Escherichia coli* 5′-methylthioadenosine/S-adenosylhomocysteine nucleosidase, *Acta Crystallogr. D 57*, 150−152.
25. Dunn, S. M., and Bryant, J. A. (1994) A Simple Spectrophotometric Assay for Plant 5′-Deoxy-5′-Methylthioadenosine Nucleosidase using Xanthine Oxidase as a Coupling Enzyme, *Phytochem. Anal. 5*, 286−290.
26. de Groot, H., and Noll, T. (1985) Enzymic determination of inorganic phosphates, organic phosphates and phosphate-liberating enzymes by use of nucleoside phosphorylase-xanthine oxidase (dehydrogenase)-coupled reactions, *Biochem. J. 230*, 255−260.
27. Allart, B., Gatel, M., Guillerm, D., and Guillerm, G. (1998) The catalytic mechanism of adenosylhomocysteine/methylthioadenosine nucleosidase from *Escherichia coli*-chemical evidence for a transition state with a substantial oxocarbenium character, *Eur. J. Biochem. 256*, 155−162.
28. Cornell, K. A., Swarts, W. E., Barry, R. D., and Riscoe, M. K. (1996) Characterization of recombinant *Escherichia coli* 5′-methylthioadenosine/S-adenosylhomocysteine nucleosidase: analysis of enzymatic activity and substrate specificity, *Biochem. Biophys. Res. Commun. 228*, 724−732.
29. Erion, M. D., Takabayashi, K., Smith, H. B., Kessi, J., Wagner, S., Honger, S., Shames, S. L., and Ealick, S. E. (1997) Purine nucleoside phosphorylase. 1. Structure−function studies, *Biochemistry 36*, 11725−11734.
30. Amyes, T. L., and Jencks, W. P. (1989) Lifetimes of Oxocarbenium Ions in Aqueous Solution from Common Ion Inhibition of the Solvolysis of α-Azido Ethers by Added Azide Ion, *J. Am. Chem. Soc. 111*, 7888−7900.
31. Fedorov, A., et al., and Almo, S. C. (2001) Transition State Structure of Purine Nucleoside Phosphorylase and Principles of Atomic Motion in Enzymatic Catalysis, *Biochemistry 40*, 853−860.
32. Singh, V., Lee, J. E., Nunez, S., Howell, P. L., and Schramm, V. L. (2005) Transition state structure of 5′-methylthioadenosine/S-adenosylhomocysteine nucleosidase from *Escherichia coli*; design principles for transition state analogues, *Biochemistry*, in press.
33. Garrett, E. R., and Mehta, P. J. (1972) Solvolysis of adenine nucleosides. I. Effects of sugars and adenine substituents on acid solvolyses, *J. Am. Chem. Soc. 94*, 8532−8541.
34. Degano, M., Almo, S. C., Sacchettini, J. C., and Schramm, V. L. (1998) Trypanosomal nucleoside hydrolase. A novel mechanism from the structure with a transition-state inhibitor, *Biochemistry 37*, 6277−6285.
35. Degano, M., Gopaul, D. N., Scapin, G., Schramm, V. L., and Sacchettini, J. C. (1996) Three-dimensional structure of the inosine-uridine nucleoside N-ribohydrolase from *Crithidia* fasciculata, *Biochemistry 35*, 5971−5981.
36. Versees, W., Decanniere, K., Van Holsbeke, E., Devroede, N., and Steyaert, J. (2002) Enzyme−substrate interactions in the purine-specific nucleoside hydrolase from Trypanosoma vivax, *J. Biol. Chem. 277*, 15938−15946.
37. Versees, W., and Steyaert, J. (2003) Catalysis by nucleoside hydrolases, *Curr. Opin. Struct. Biol. 13*, 731−738.
38. Humphrey, W., Dalke, A., and Schulten, K. (1996) VMD-visual molecular dynamics, *J. Mol. Graph. 14*, 33−38.

BI050493Q